High-Entropy Alloy CoCrFeMnNi Produced by Powder Metallurgy

Nadine Eißmann, Burghardt Klöden, Thomas Weißgärber, Bernd Kieback

World PM2016, Hamburg, 9-13 October 2016

TECHNISCHE UNIVERSITÄT DRESDEN

Fraunhofer IFAM Institutsteil Dresden

Content

1. Fundamentals and Motivation
2. Powder Manufacturing
3. Pressureless Sintering (MIM)
4. Spark Plasma Sintering
5. Electron Beam Melting
6. Comparison Production Methods
7. Summary and Outlook

1. Fundamentals and Motivation

High-Entropy Alloys (HEAs):

- 5 principal elements, each 5 till 35 at%
- Minor elements, below 5 at%

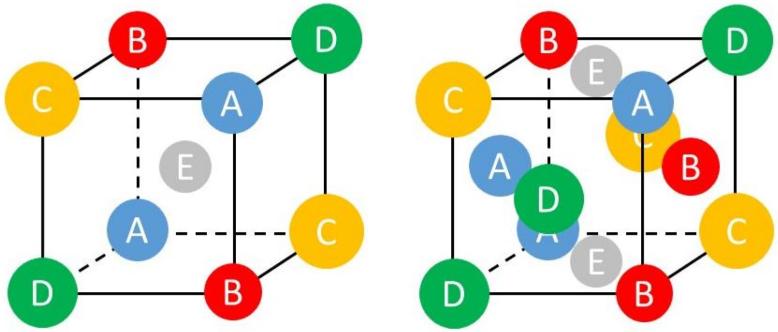

Crystal structure of HEAs

Properties

- Simple solid solution phases
- High hardness and strength
- Good thermal stability
- Excellent corrosion, wear and oxidation resistance

Applications

- Tools, molds, dies, mechanical and furnace parts
- Anticorrosive high-strength materials in chemical plants, and IC foundries
- Functional coatings and diffusion barriers

1. Fundamentals and Motivation

Core Effects in High-Entropy Alloys

High-Entropy Effect

$$\Delta S_{mix} = -R \sum_{i=1}^{n} X_i \ln X_i$$

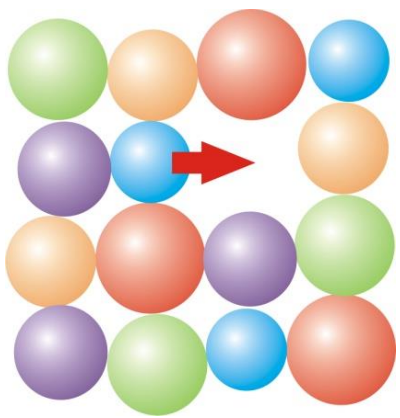

Sluggish Diffusion Effect

Lattice Distortion Effect

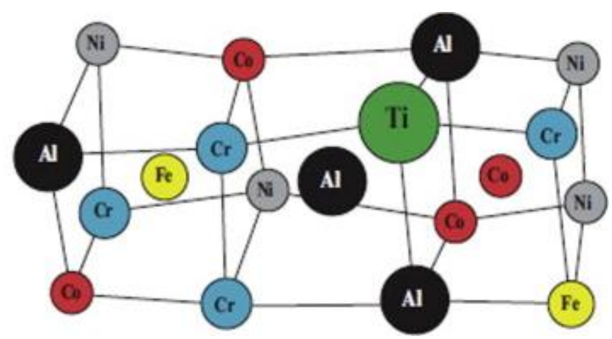

[1]

1. Fundamentals and Motivation

Core Effects - High-Entropy Effect

$$\Delta S_{mix} = -R \sum_{i=1}^{n} X_i \ln X_i$$

Assumption:

- Entropy of mixing ΔS_{mix} stabilises solid solution phases
  - ⇨ Origin of the name

Experimental results:

- Phase analysis shows also amorphous and intermetallic phases
- Entropy of mixing not sufficient for stability of HEAs

⇨ Further thermodynamic parameters (enthalpy of mixing ΔH_{mix}, atomic size different δ, …) under intense investigation

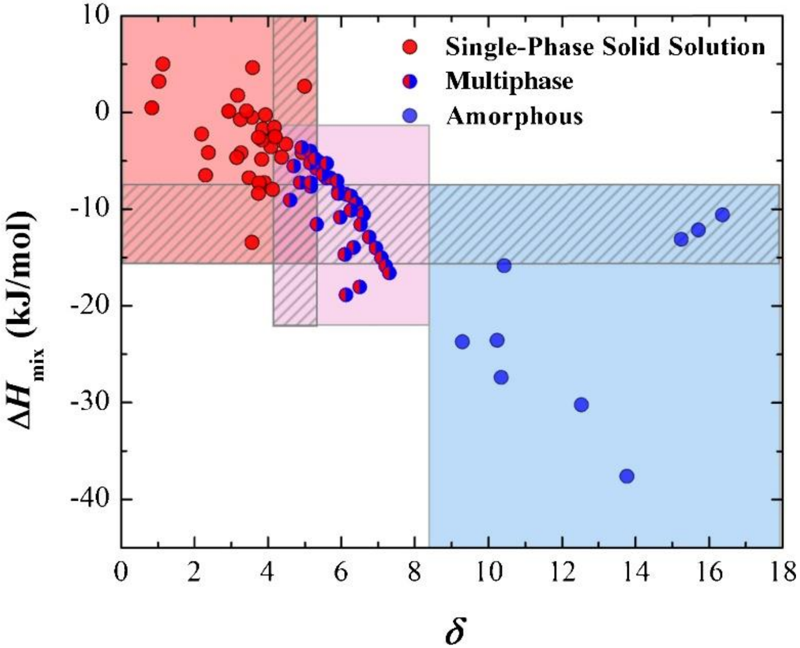

Influence of thermodynamic parameters on resulting microstructure [2]

1. Fundamentals and Motivation

Core Effects - Sluggish Diffusion Effect

Assumption:

- Sluggish diffusion in HEAs
- *Mobility of atoms: HEAs < steel < raw metals*

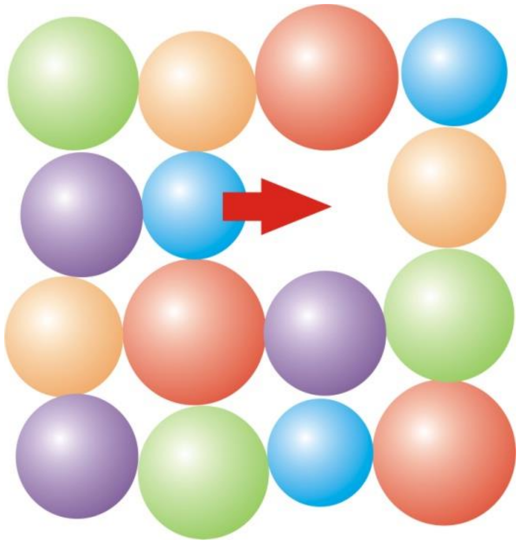

Diffusion in HEAs

Experimental results:

- Different bonding configuration dependent on lattice site
- *Lattice potential energy* LPE varies depending on the lattice site
  - ⇨ LPE low → traps

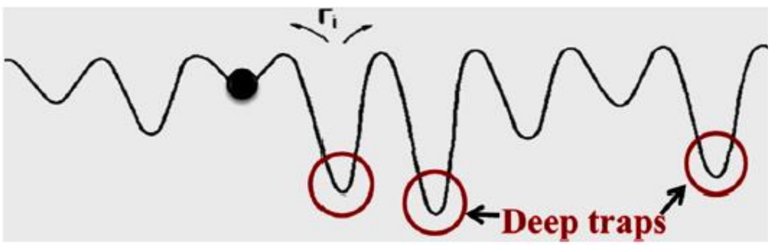

Fluctuation of LPE for diffusion path of atoms in HEAs [3]

Consequences:

- Influence on all diffusion-controlled processes
  - ⇨ Metastable phases
  - ⇨ Slow grain growth
  - ⇨ Nano precipitations

1. Fundamentals and Motivation

Core Effects - Sluggish Diffusion Effect

- ⇨ First diffusion research by *Tsai et al.* (2013) for $CoCrFeMn_{0.5}Ni$ HEA

$$D = D_0 e^{-\frac{Q}{RT}}$$

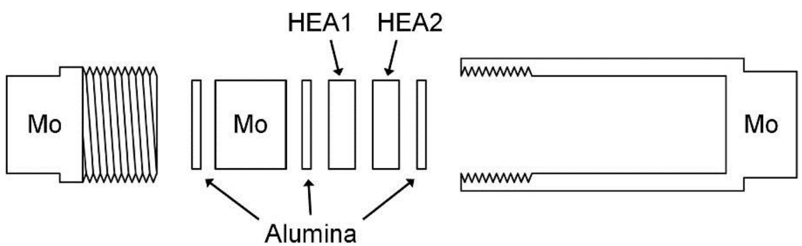

*Schematic diagram showing the assembly of the diffusion couples (*900, 950, 1000 and 1050°C) *[4]*

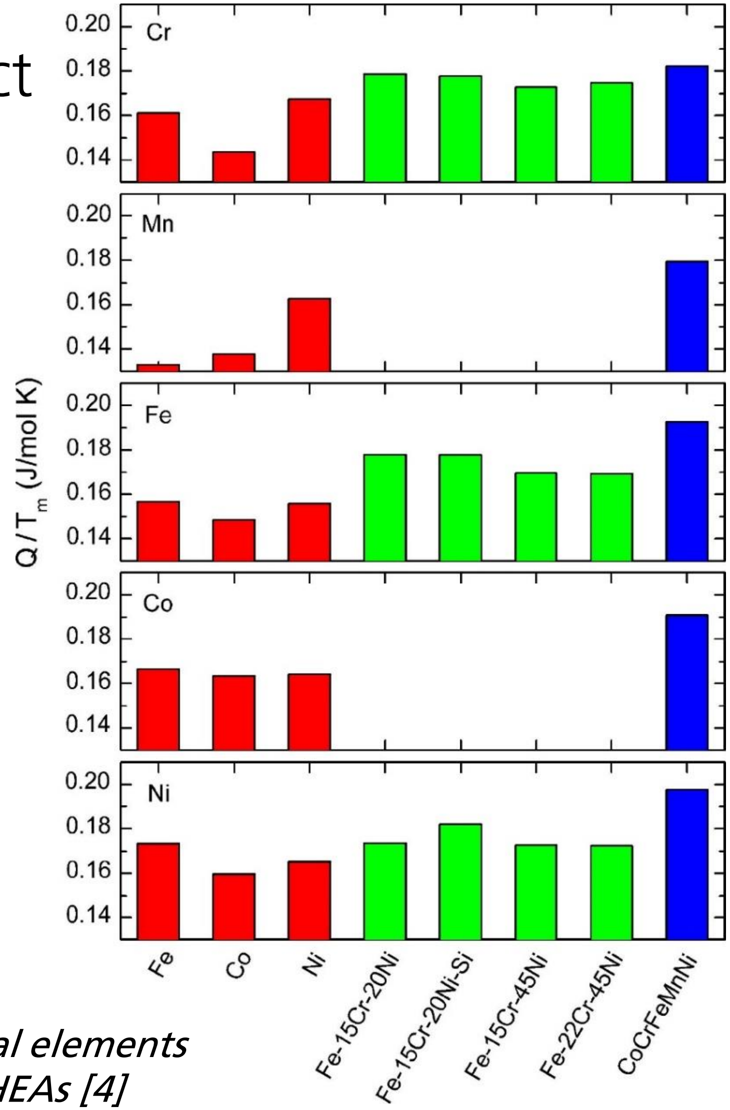

Activation energy for several elements in conventional alloys and HEAs [4]

1. Fundamentals and Motivation

Core Effects - Lattice Distortion Effect

Assumption:

- Varying atomic sizes cause severe distortions
- No difference between matrix and solute atoms

Consequences: Influence on properties

- Impeding of dislocation motion
  ⇨ Solid solution strengthening
  - High hardness
  - E.g.: MoNbTaVW → HV 530

- Electron and phonon scattering
  ⇨ Electrical and thermal conductivity are low

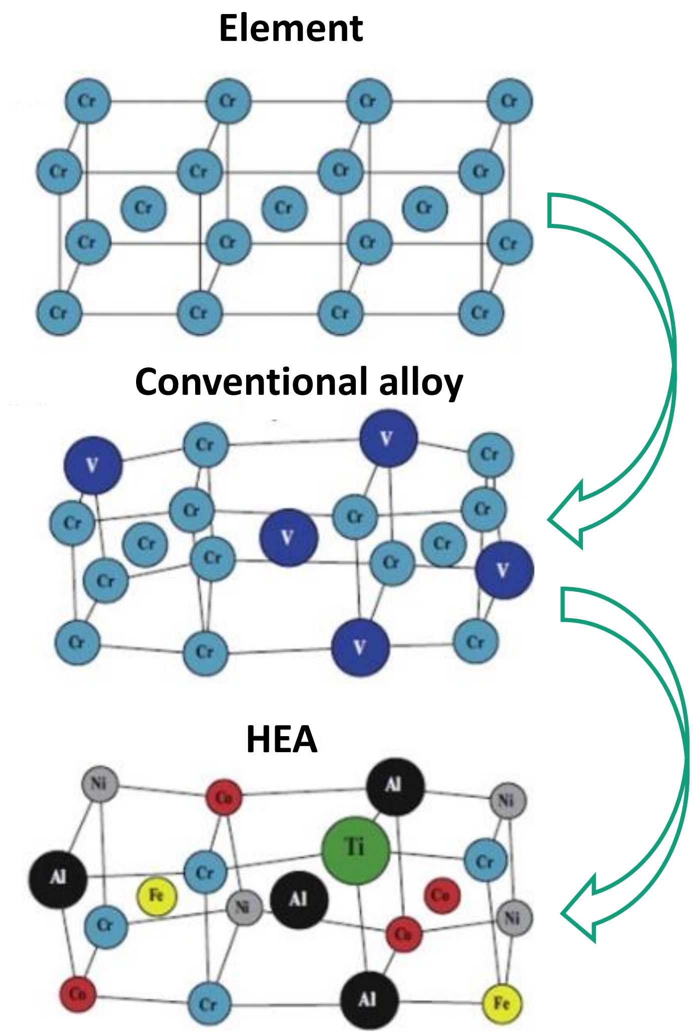

Lattice distortion in elements, conventional alloys and HEAs [1]

1. Fundamentals and Motivation

Core Effects - Summary

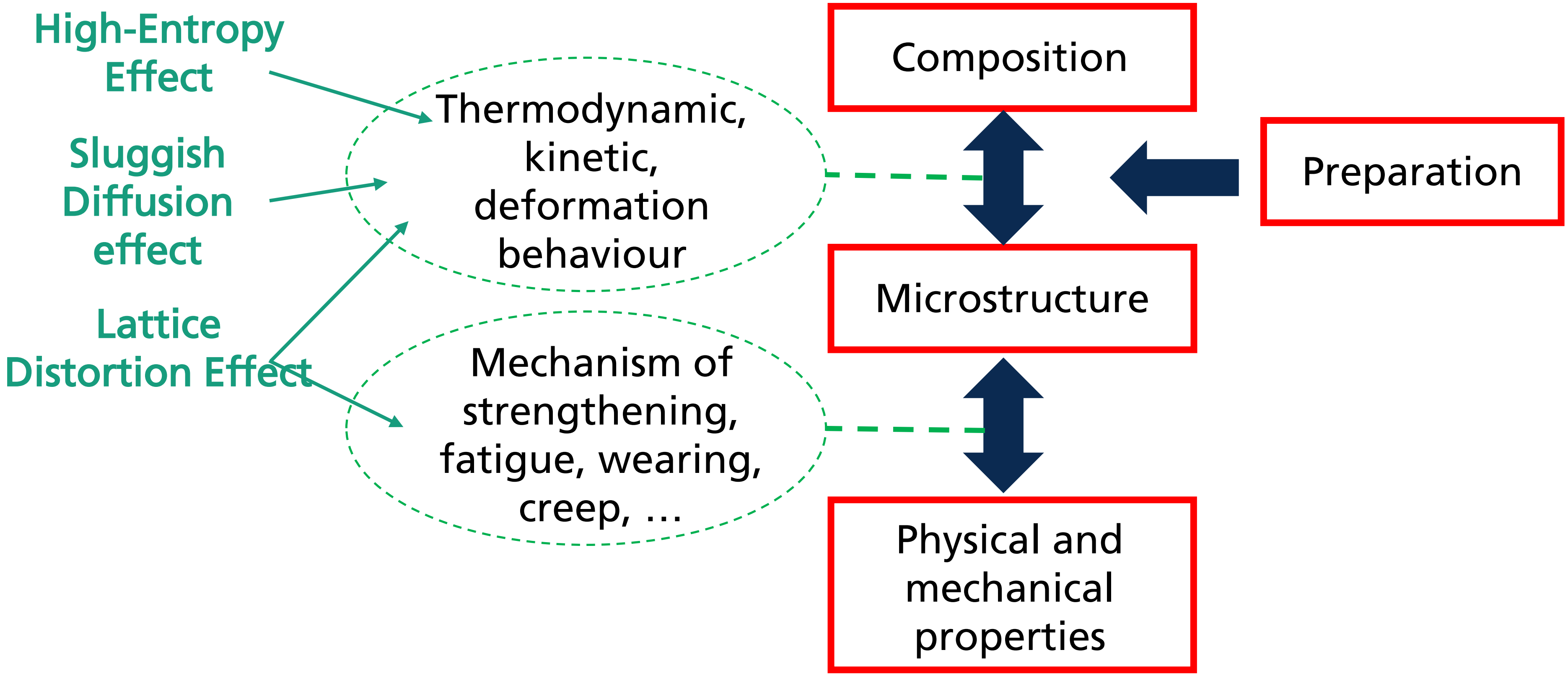

[3]

1. Fundamentals and Motivation

World of High-Entropy Alloys

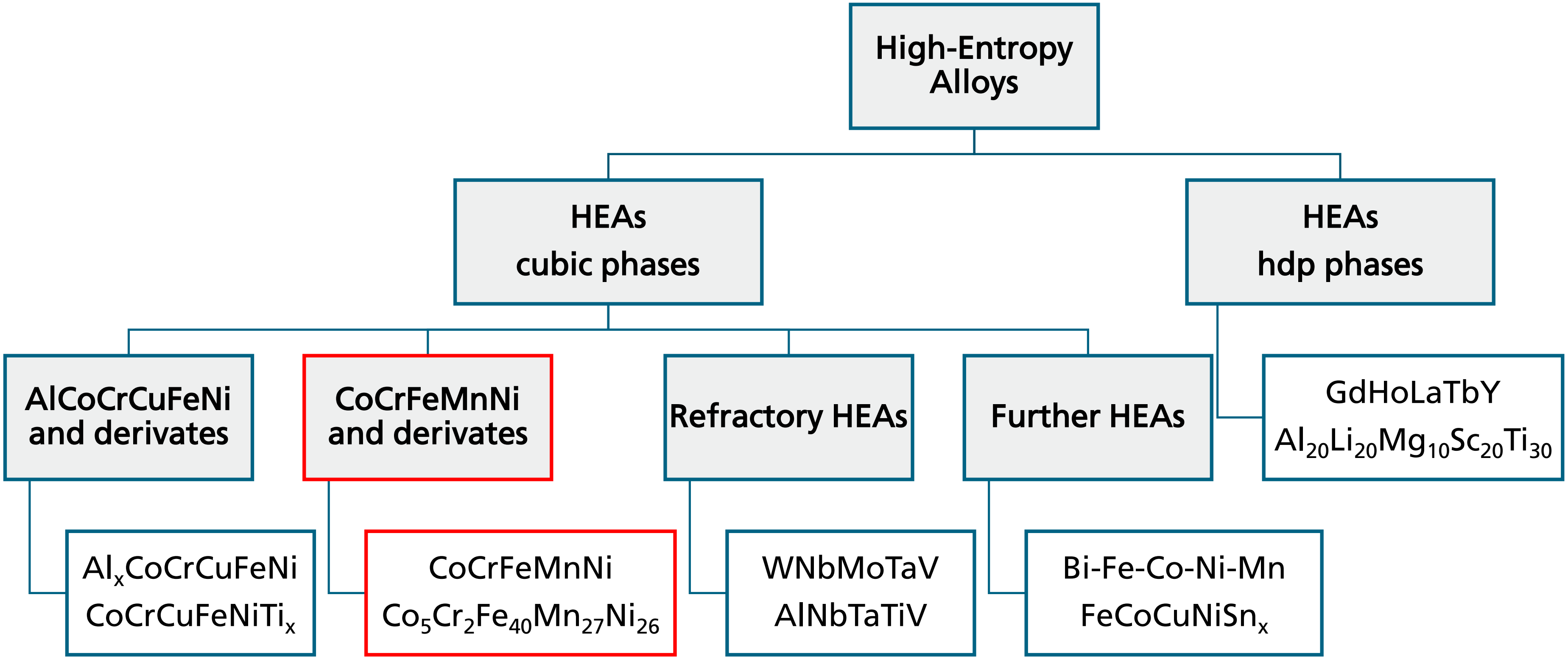

Powder Metallurgical Preparation of CoCrFeMnNi

Gas atomisation of CoCrFeMnNi

↓

Powder characterisation and preparation

↓ ↓ ↓

Pressureless sintering (MIM)	Spark Plasma Sintering (SPS)	Selective Electron Beam Melting (EBM)

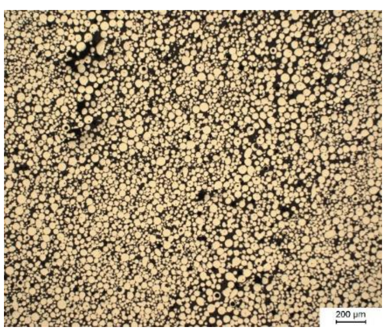

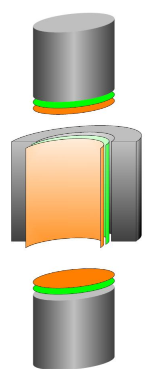

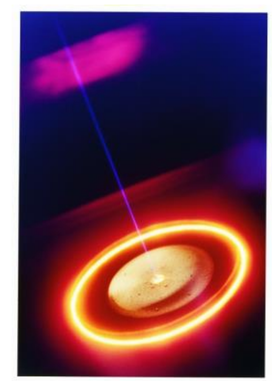

[5]

2. Powder Manufacturing

Argon Gas Atomisation

Atomisation facility [6]

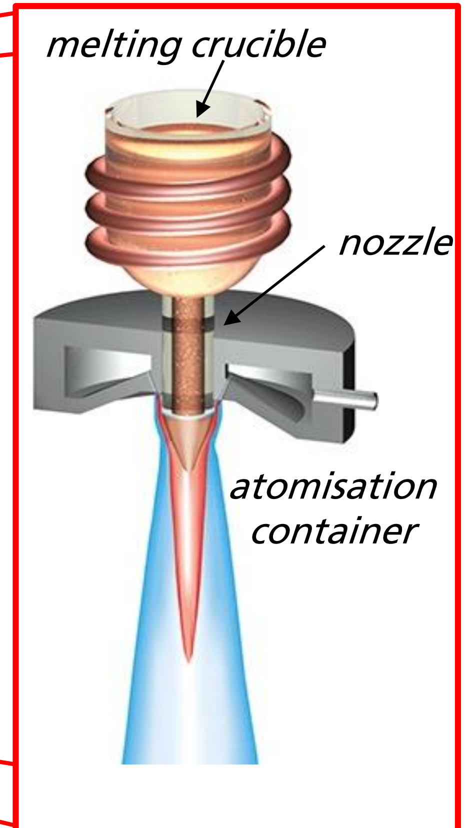

Atomisation principle [7]

- Argon gas atomisation (*Fraunhofer UMSICHT)*
- Starting material: Mixture of raw elements
- Atomising of melt by compressed argon

2. Powder Manufacturing

Powder Characterisation of CoCrFeMnNi

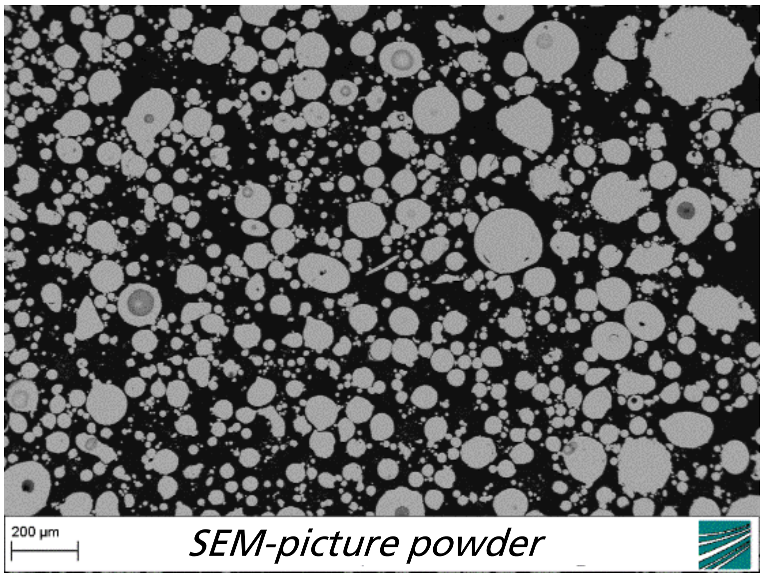

SEM-picture powder

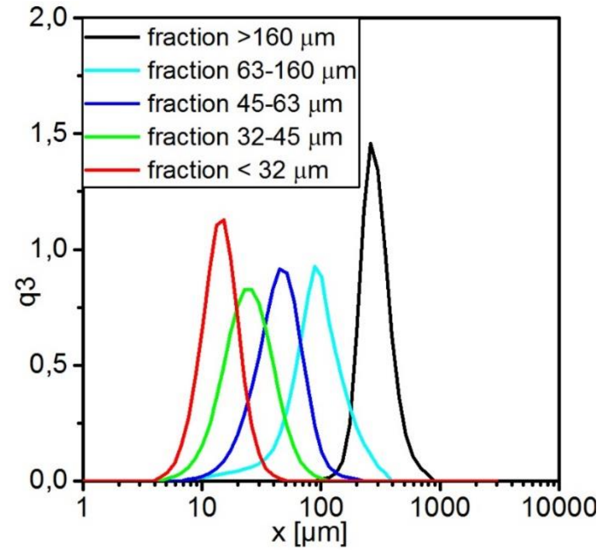

Particle size distribution after sieving process

EDS-analysis powder

at-%	Cr	Mn	Fe	Co	Ni
Pulver	20,2	20,2	19,7	19,8	20,1
He et al. [5]	21,3	20,7	19,4	19,3	19,3
SOLL	**20**	**20**	**20**	**20**	**20**

CoCrFeMnNi powder

- Single phase microstructure
- Ideal composition

3. Pressureless Sintering (MIM)

Sintering of Lose Powders

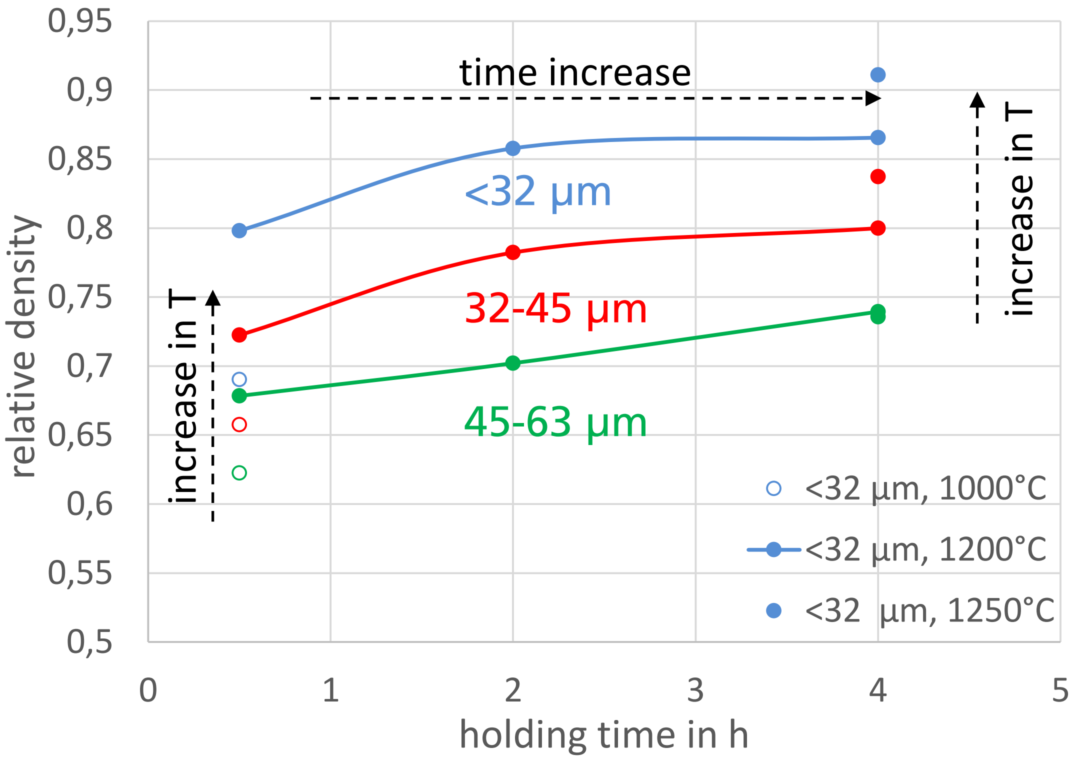

Influence of sintering time on density (1200°C)

- Increase in sintering time followed by an increase in relative density ρ/ρ_{theo}
- Densities ρ/ρ_{theo} > 85% for finest powder

Finest powder fractions [8]

Heat treatment

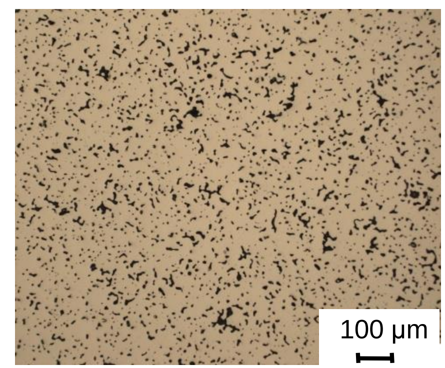

Resulting microstructure

3. Pressureless Sintering (MIM)

Sedimentation Process

Finest powder fractions [8]

Binder [9]

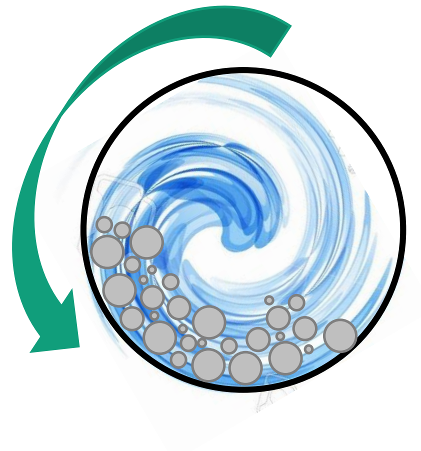

Speedmixing

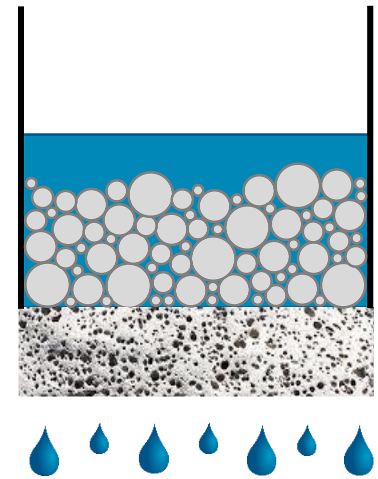

Sedimentation

3. Pressureless Sintering (MIM)

Dilatometry of Sedimentation Samples

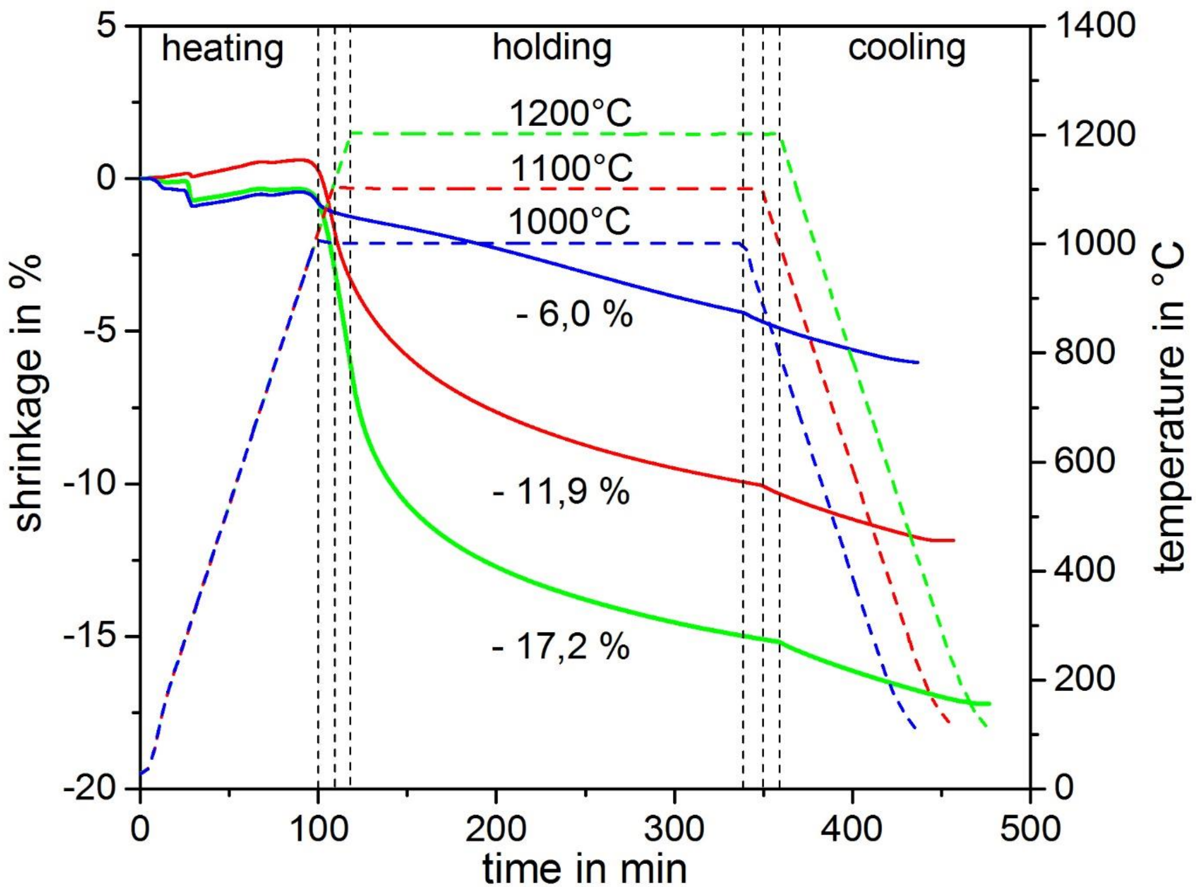

Results of dilatometry at different holding temperatures (10 K/min, 4 h)

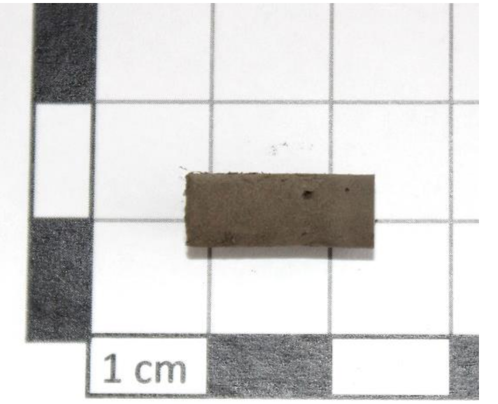

resulting sample

- Usage of smallest powder fractions
- Considerable shrinkage detected
- "Jump" during heating due to debinding of powder
- Debinding finished at 600°C

3. Pressureless Sintering (MIM)

Sintering of Homogeneous Solid Solutions

Homogeneous solid solution A_xB_y ($D_A \gg D_B$)

Initial stage

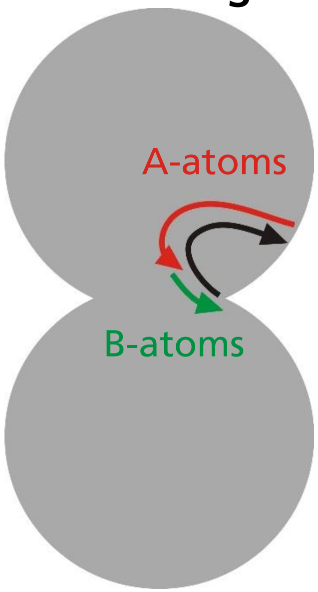

Final stage

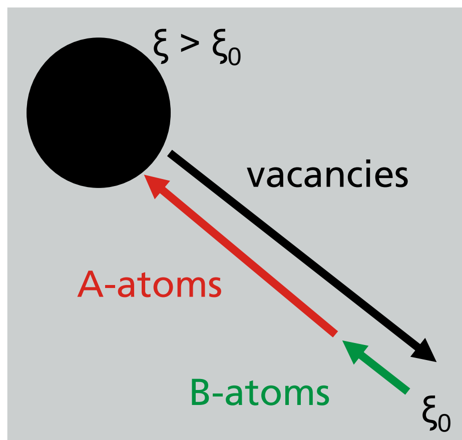

$$c_A(R) = c_A^0 \left[1 - \frac{D_B}{D_B \cdot c_A + D_A \cdot c_B} \Delta\xi \Big|_{r=R} \right]$$

$$\Delta c_A \Big|_{r=R} = c_A(R) - c_A^0 = - \frac{c_A^0 D_B}{D_B \cdot c_A + D_A \cdot c_B} \Delta\xi \Big|_{r=R}$$

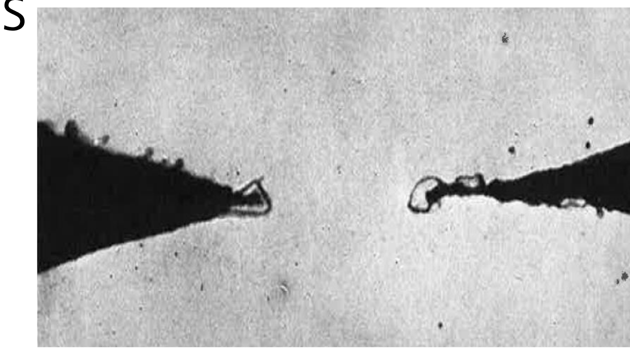

Etched neck region between two Cu-wires with 8 at% In [10]

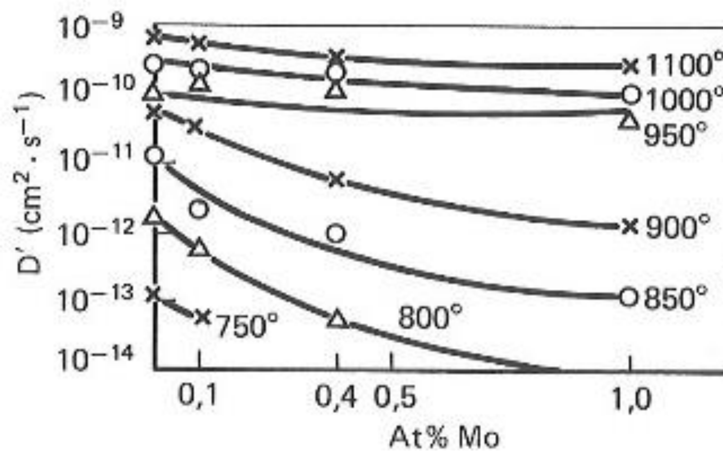

Influence of alloy composition in Fe-Mo alloys on mobility coefficient D′ [11]

TECHNISCHE UNIVERSITÄT DRESDEN

Fraunhofer IFAM Institutsteil Dresden

4. Spark Plasma Sintering (SPS)

Varying particle sizes [8]

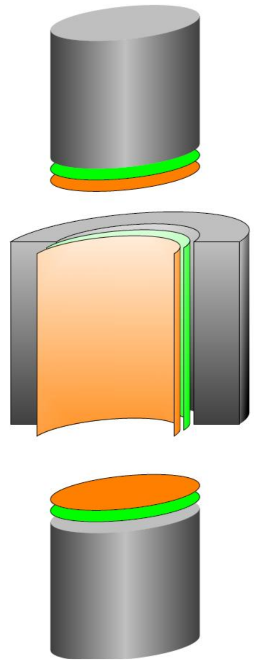

SPS-die

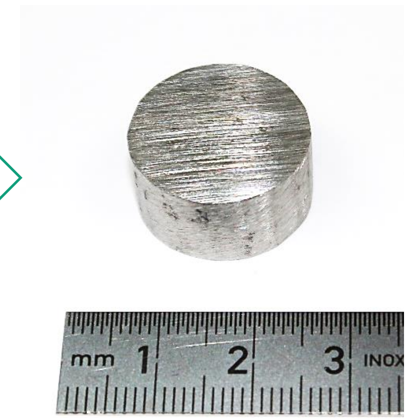

Resulting sample

- Varying particle sizes
- SPS at 1000°C, 55 MPa, Ø 20-30 mm for 10 min
- Application of graphite and tungsten foil

4. Spark Plasma Sintering (SPS)

Microstructure Characterisation

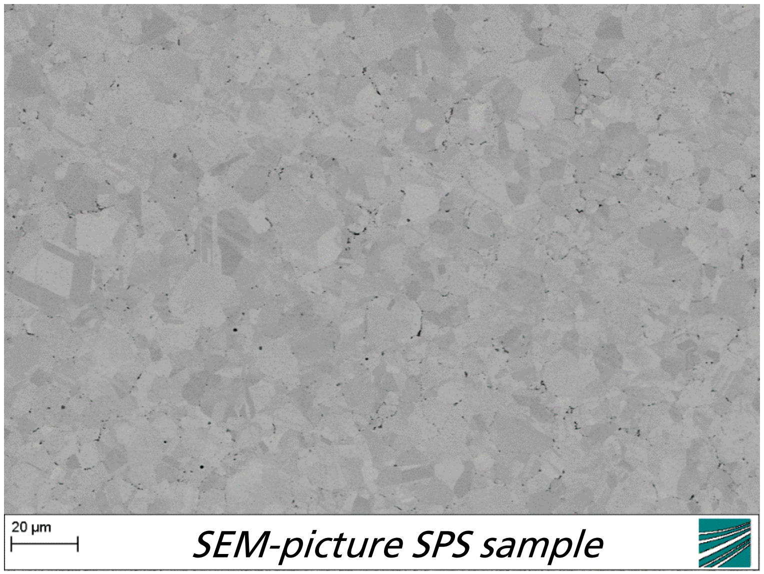

SEM-picture SPS sample

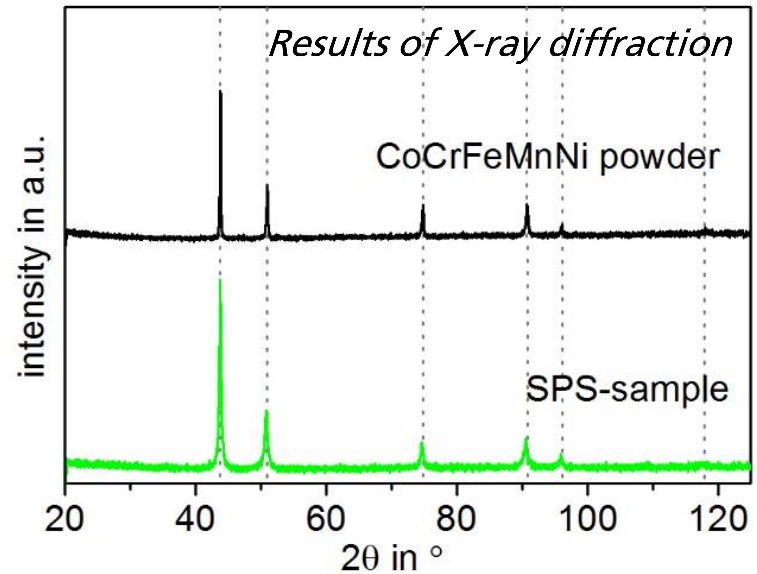

EDS-analysis powder

at-%	Cr	Mn	Fe	Co	Ni
Pulver	20,2	20,2	19,7	19,8	20,1
SPS-Probe	20,3	19,7	20,0	20,1	19,9
He et al. [5]	21,3	20,7	19,4	19,3	19,3
SOLL	**20**	**20**	**20**	**20**	**20**

SPS sample

- Ideal composition
- Single phase microstructure

4. Spark Plasma Sintering (SPS)

EDS-Mapping

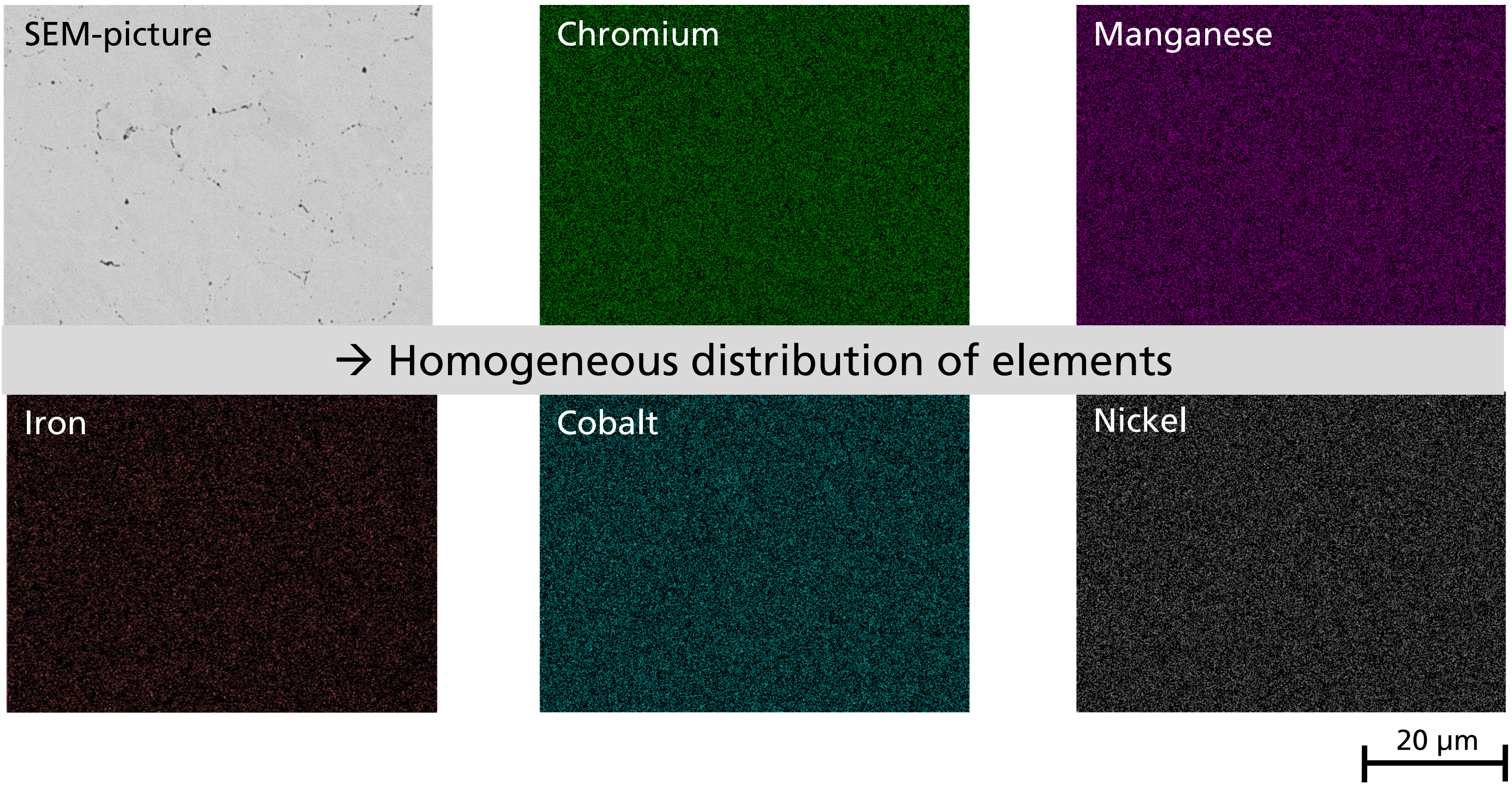

→ Homogeneous distribution of elements

4. Spark Plasma Sintering (SPS)

Mechanical Properties - 3-Point-Bending Test

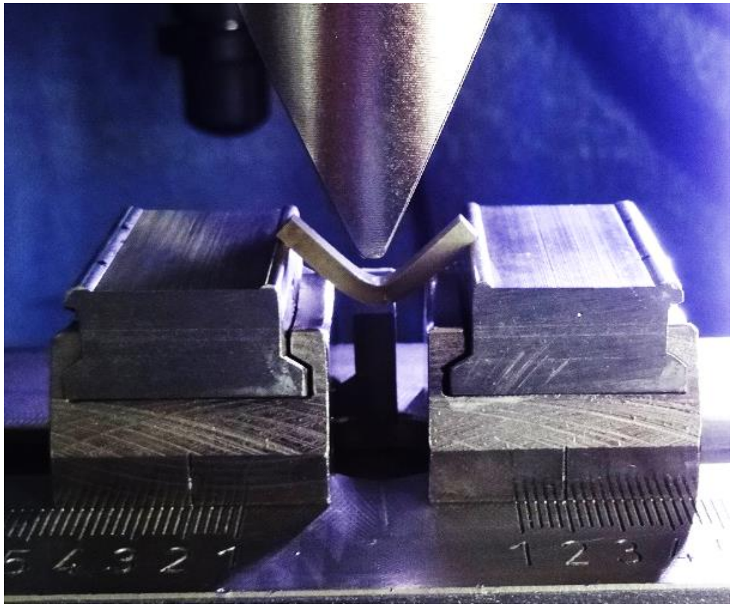

Testing facility

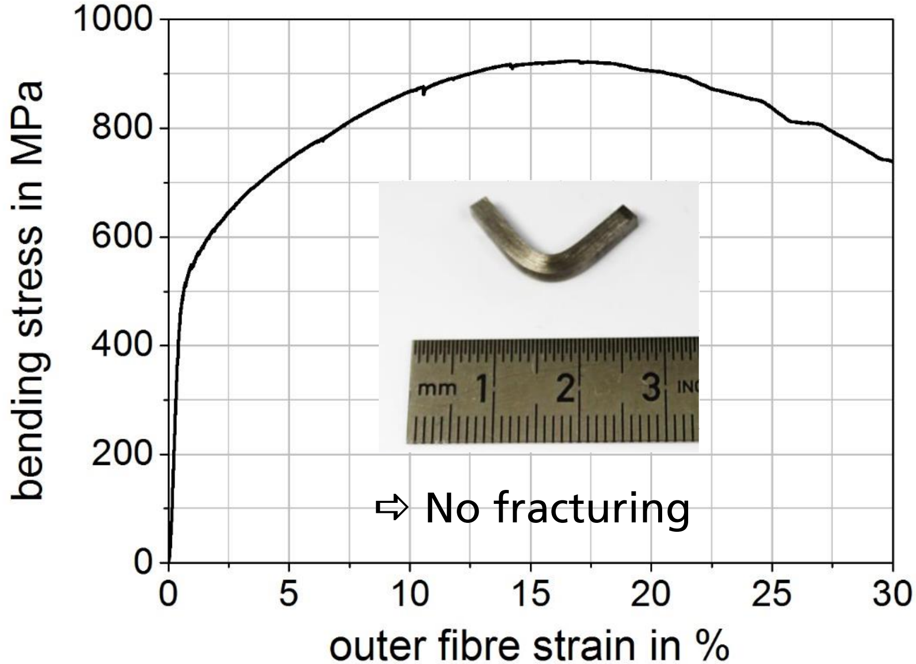

Results 3-point-bending test

Bending test:
(25 mm x 2,5 mm x 2,5 mm)

- Outer fibre strain at F_{max}: 16,18 %
- Max. outer fibre strain : > 30 %
- Bending strength: 920 MPa

4. Spark Plasma Sintering (SPS)

Mechanical Properties - Tensile Test

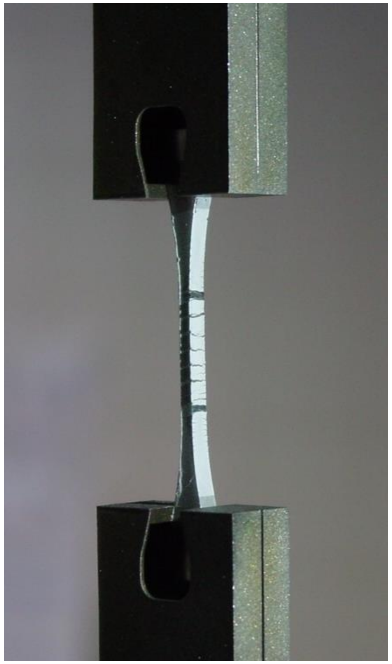

Testing facility

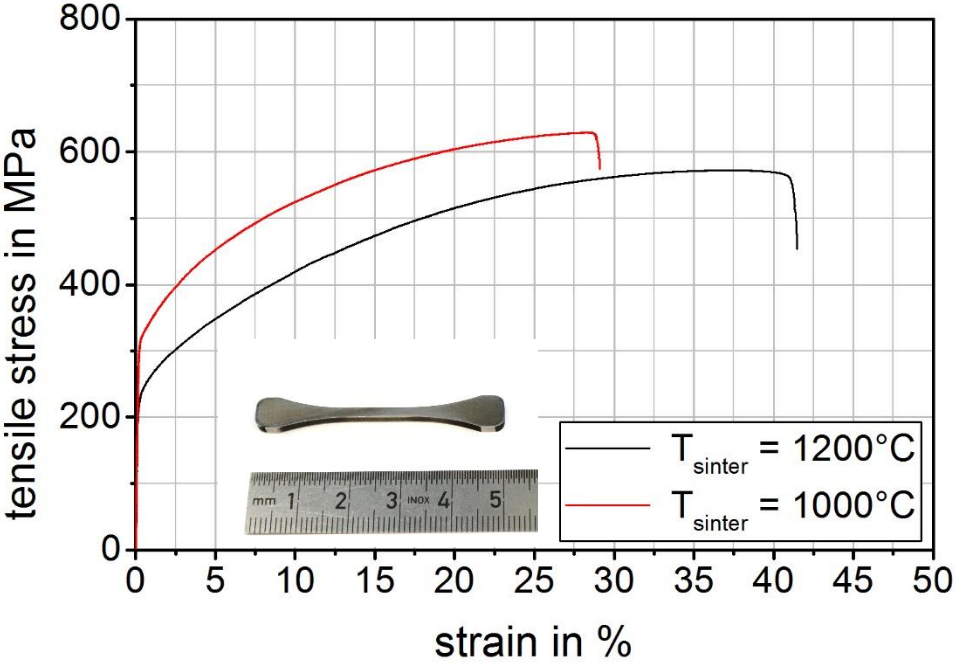

Results tensile test

Tensile testing:
(50 mm x 2,5 mm x 2 mm)

- Yield strength: 310 MPa
- Tensile strength: 610 MPa
- Elongation at fracture: 27 %

4. Spark Plasma Sintering (SPS)

Mechanical Properties - Summary

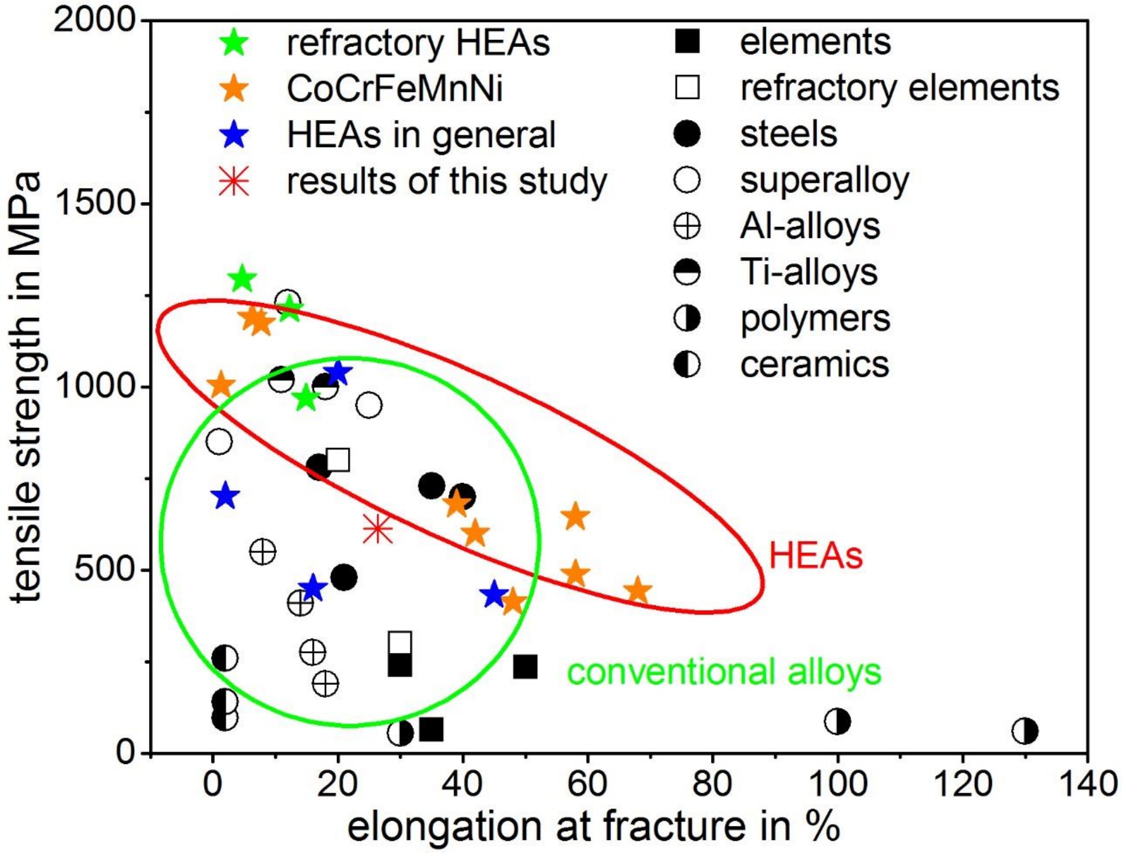

Stress-strain- diagram for various conventional materials and HEAs [12-43]

- HEAs can show superior mechanical properties than conventional alloys
- Results of this study fit literature values

TECHNISCHE UNIVERSITÄT DRESDEN

Fraunhofer IFAM Institutsteil Dresden

5. Selective Electron Beam Melting (SEBM)

Principles and Basics

- Powder-bed-based technique
- High beam power
  - ⇨ High-melting materials
- Fast beam deflection
  - ⇨ High building rates
- Vacuum
  - ⇨ Reactive materials
- Pre-heating of powder bed
  - ⇨ Minimising of thermal stresses
  - ⇨ Few supporting structures

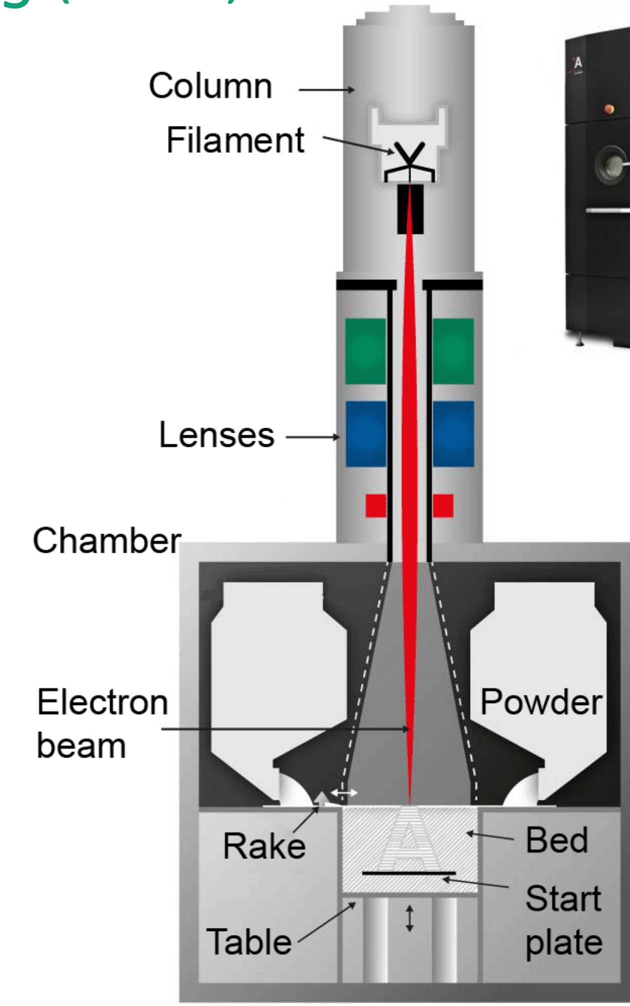

SEBM principle und EBM-Anlage [44, 45]

5. Selective Electron Beam Melting (SEBM)

SEBM-Process

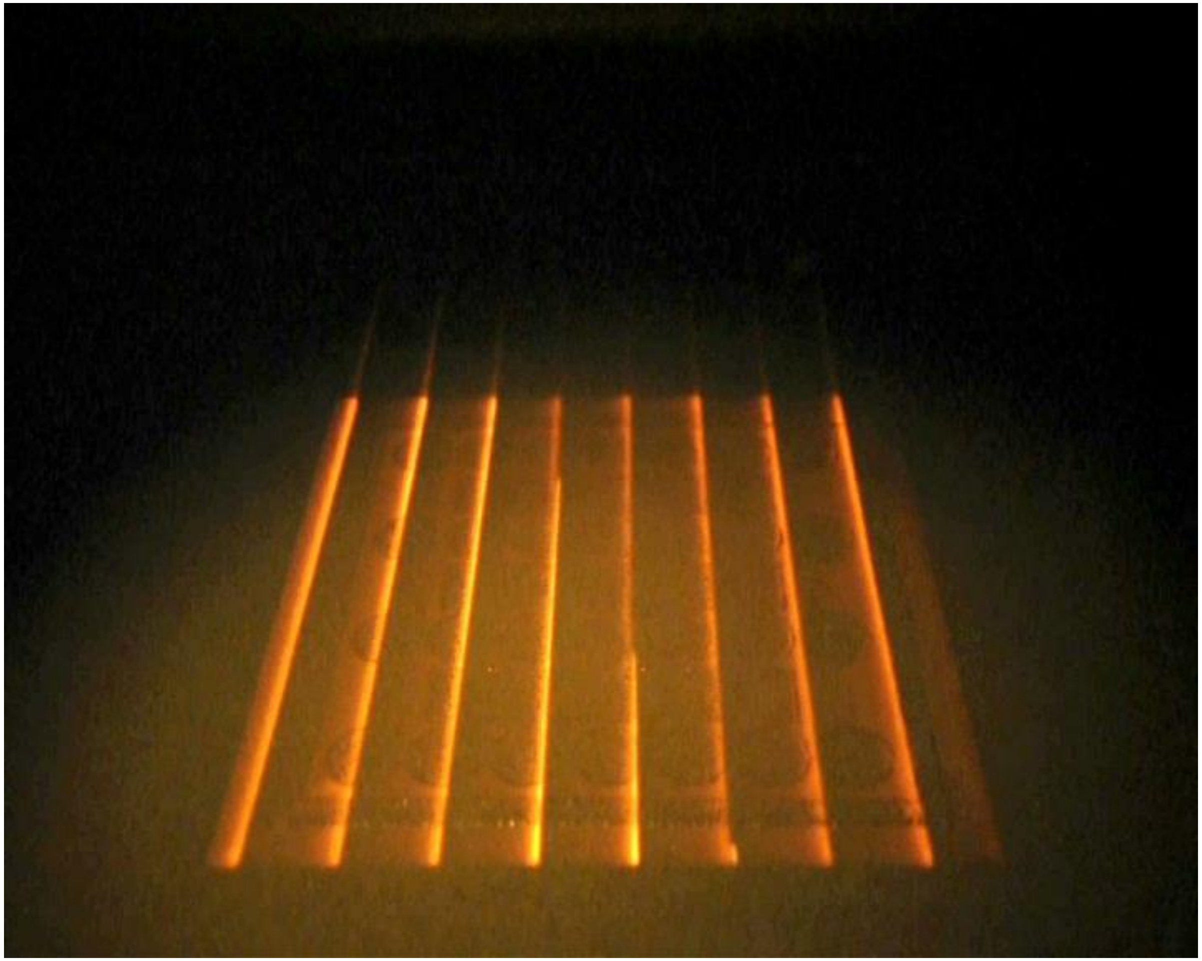

5. Selective Electron Beam Melting (SEBM)

SEBM-Samples

- Evaporation of manganese (up to 2 m%)
  - ⇨ No change in crystal structure
- Resulting density up to $\rho \approx 97\%$
  - ⇨ Depending on final composition

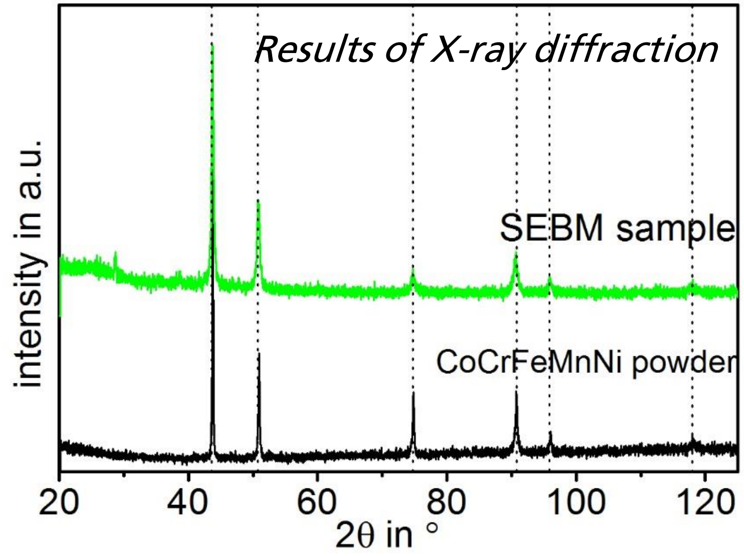

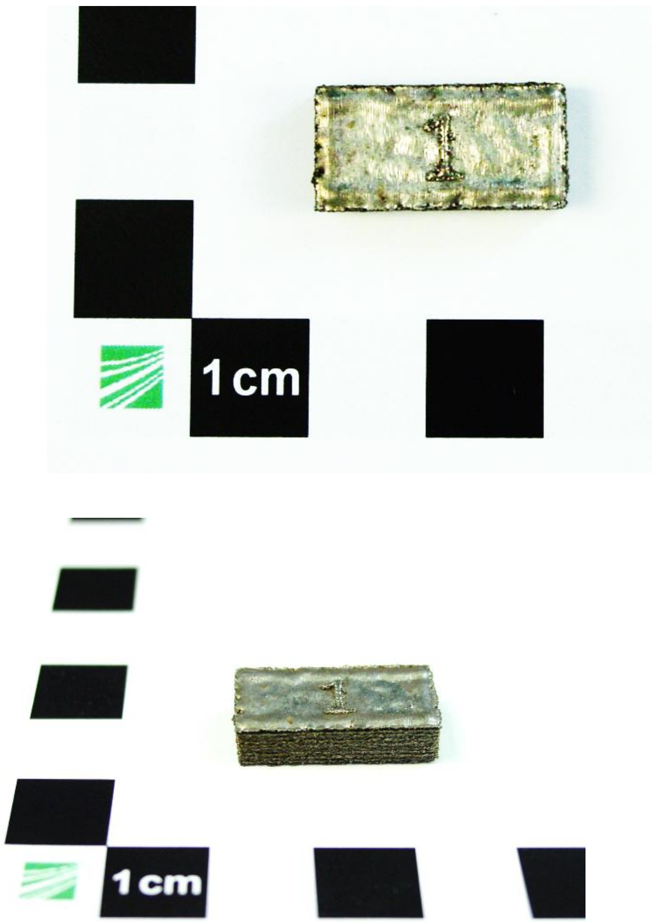

HEA-SEBM-samples

5. Selective Electron Beam Melting (SEBM)

SEBM-Microstructure

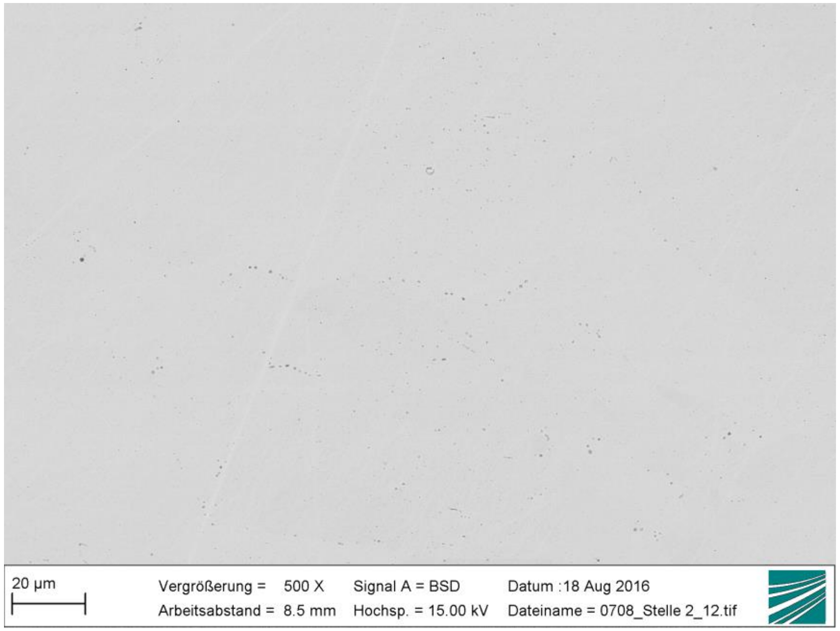

at-%	Cr	Mn	Fe	Co	Ni
powder	20,2	20,2	19,7	19,8	20,1
EBM	20,4	18,7	20,1	20,3	20,5
He et al. [5]	21,3	20,7	19,4	19,3	19,3
SOLL	**20**	**20**	**20**	**20**	**20**

EBM sample

- Composition: Mn deviation (evaporation)
- Single phase microstructure

5. Selective Electron Beam Melting (SEBM)

EDS mapping

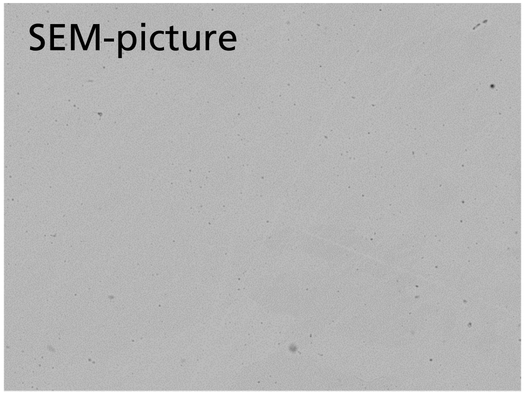

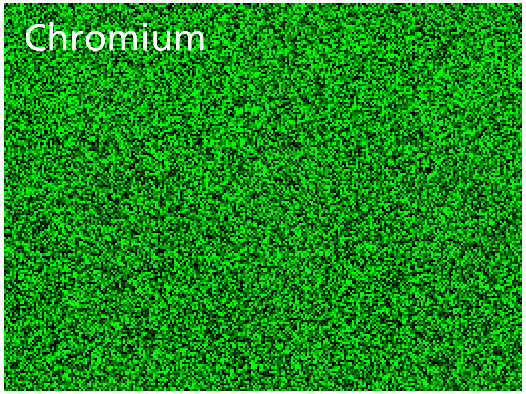

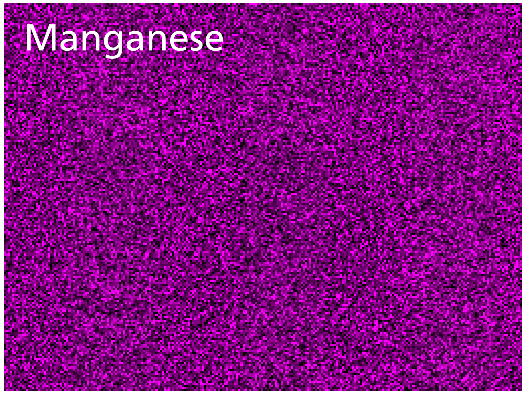

→ Homogeneous distribution of elements

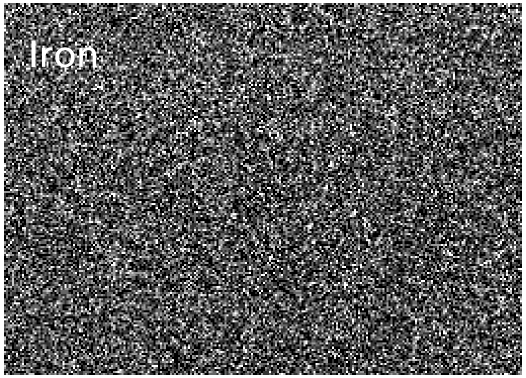

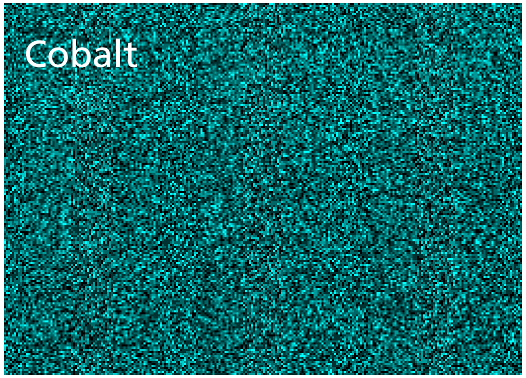

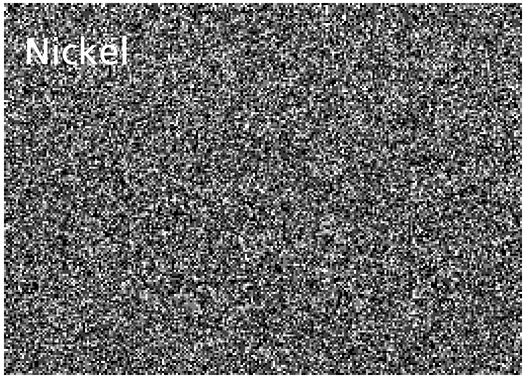

6. Comparison Powder Metallurgical Methods

Argon Gas Atomisation

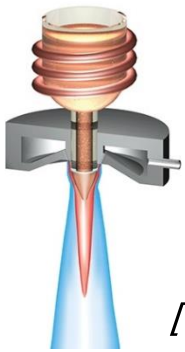

[7]

- ✓ Homogeneous and single-phase powders
- ✓ Industrial relevant amount of powder

- – Not suitable for all materials and alloys (refractory alloys, etc.)

Pressureless Sintering (MIM)

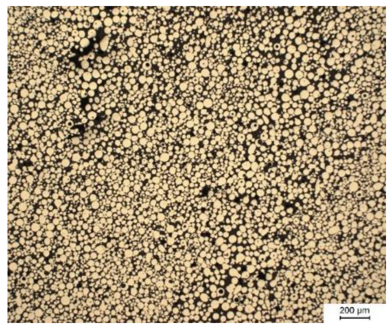

- ✓ Near-net-shape components
- ✓ Analysis of sintering regime

- – ↑ Process time

Spark Plasma Sintering

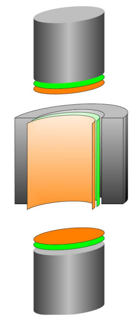

- ✓ ↓ Process time
- ✓ Homogeneous microstructure
- ✓ Density ≈ 99 %

- – Limited geometrical possibilities

Selctive Electron Beam Melting

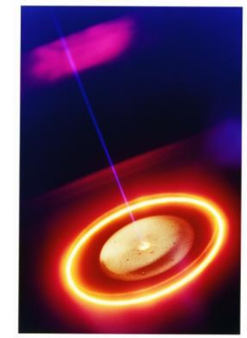

[5]

- ✓ Complex shapes
- ✓ Homogeneous microstructure
- ✓ Density up to 97%

- – ↑ Process time
- – Evaporation

7. Summary and outlook

- Powder metallurgy highly suitable for HEA production
- *Powder Production:* gas atomisation
  - ⇨ Homogeneous and spherical powders
  - ⇨ Suitable for industrial application
- *Compaction:*
  - Pressureless Sintering
    - ⇨ Density up to 90%
    - ⇨ No decomposition
  - Spark Plasma Sintering
    - ⇨ Homogeneous and ideal microstructure
    - ⇨ Density up to 99%
  - Electron Beam Melting
    - ⇨ Density up to 97 %
    - ⇨ Evaporation

Thank you for your attention!

References

[1] Y. Zhang, T. T. Zuo, Z. Tang, M. C. Gao, K. A. Dahmen, P. K. Liaw, und Z. P. Lu, „Microstructures and properties of high-entropy alloys“, *Prog. Mater. Sci.*, Bd. 61, S. 1–93, Apr. 2014.

[2] Y. F. Ye, Q. Wang, J. Lu, C. T. Liu, und Y. Yang, „High-entropy alloy: challenges and prospects“, *Mater. Today*, In Press, Corrected Proof.

[3] J.-W. Yeh, „Physical Metallurgy of High-Entropy Alloys“, *JOM*, Bd. 67, Nr. 10, S. 2254–2261, Aug. 2015.

[4] K.-Y. Tsai, M.-H. Tsai, und J.-W. Yeh, „Sluggish diffusion in Co–Cr–Fe–Mn–Ni high-entropy alloys“, *Acta Mater.*, Bd. 61, Nr. 13, S. 4887–4897, Aug. 2013.

[5] „Press material and contact - Arcam Group“. [Online]. Verfügbar unter: http://www.arcamgroup.com/about-arcam/press-material-and-contact/. [Zugegriffen: 26-Juli-2016].

[6] „ATZ Entwicklungszentrum“, *Bayern Innovativ*. [Online]. Verfügbar unter: http://bayern-innovativ.de/e308b339-5dbf-19b8-a01e-917db1a74684?PP=625abfc6-f7db-33b2-ef72-e2dca23fd539. [Zugegriffen: 20-Nov-2014].

[7] „AIMResearch - research highlights - Bulk metallic glasses: Nanowire gems in the particle dust“. [Online]. Verfügbar unter: https://research.wpi-aimr.tohoku.ac.jp/eng/research/681. [Zugegriffen: 31-Juli-2015].

[8] Arcam AB, „Metal Powders“, *Arcam AB*. [Online]. Verfügbar unter: http://www.arcam.com/technology/products/metal-powders/. [Zugegriffen: 26-Juli-2016].

References

[9] Umwelt Bundesamt, „Die Umsetzung von REACH“, *Umweltbundesamt*, 07-Sep-2012. [Online]. Verfügbar unter: http://www.umweltbundesamt.de/themen/chemikalien/chemikalien-reach/die-umsetzung-von-reach. [Zugegriffen: 26-Juli-2016].

[10] G. C. Kuczynski, G. Matsumura, und B. D. Cullity, „Segregation in homogeneous alloys during sintering“, *Acta Metall.*, Bd. 8, Nr. 3, S. 209–215, März 1960.

[11] F. Thümmler, „Planseeber. f. Pulvermetallurgie 6“, 2, 1958.

[12] Wolfram Industrie, Tungsten Technology Germany, „W und Mo: Daten und Technik“. [Online]. Verfügbar unter: http://www.wolfram-industrie.de/downloads/Daten%20und%20Technik%20deutsch.pdf?PHPSESSID=20f22143ec72fe3afcef2d8c7cc440fe. [Zugegriffen: 28-Apr-2016].

[13] Wilhelm Herm. Müller GmbH & Co.Kg, „Werkstoffdatenblatt PC transparent“. [Online]. Verfügbar unter: http://www.whm.net/content/de/download/res/14481-3.pdf. [Zugegriffen: 28-Apr-2016].

[14] Deutsche Edelstahlwerke, „Unlegierter Vergütungsstahl 1.1191/1.1201: C45E/C45R“. [Online]. Verfügbar unter: http://www.dew-stahl.com/fileadmin/files/dew-stahl.com/documents/Publikationen/Werkstoffdatenblaetter/Baustahl/1.1191_1.1201_de.pdf. [Zugegriffen: 28-Apr-2016].

[15] Brandenburgische Technische Universität Cottbus, „Titan und Titanlegierungen“. [Online]. Verfügbar unter: http://www-docs.tu-cottbus.de/metallkunde/public/files/Skripte/SS2012-LBW-Titan.pdf. [Zugegriffen: 28-Apr-2016].

References

[16] ThyssenKrupp, „Titan Grade 5“. [Online]. Verfügbar unter: http://www.thyssenkrupp.ch/documents/Titan_Grade_5.pdf. [Zugegriffen: 28-Apr-2016].

[17] A. Gali und E. P. George, „Tensile properties of high- and medium-entropy alloys“, *Intermetallics*, Bd. 39, S. 74–78, Aug. 2013.

[18] WHS Sondermetalle, „Tantal (Ta, TaW2.5, TaW10)“. [Online]. Verfügbar unter: http://www.whs-sondermetalle.de/pdf/Tantal_web.pdf. [Zugegriffen: 28-Apr-2016].

[19] M. J. Jiří Zýka, „STRUCTURE AND MECHANICAL PROPERTIES OF TaNbHfZrTi HIGH ENTROPY ALLOY“, 2015.

[20] ThyssenKrupp -Schulte, „S235Jxx: Werkstoffdatenblatt.“ [Online]. Verfügbar unter: http://www.thyssenkrupp-schulte.de/tl_files/ThyssenKrupp/Infothek%20(Downloads)/Baustaehle/S235Jxx.pdf. [Zugegriffen: 28-Apr-2016].

[21] Y. Liu, J. Wang, Q. Fang, B. Liu, Y. Wu, und S. Chen, „Preparation of superfine-grained high entropy alloy by spark plasma sintering gas atomized powder“, *Intermetallics*, Bd. 68, S. 16–22, Jan. 2016.

[22] Deutsche Edelstahlwerke, „Nichtrostender superaustenitischer Nickel- Chrom-Molybdän-Kupfer-Stahl: 1.4539“. [Online]. Verfügbar unter: http://www.dew-stahl.com/fileadmin/files/dew-stahl.com/documents/Publikationen/Werkstoffdatenblaetter/RSH/1.4539_de.pdf. [Zugegriffen: 28-Apr-2016].

References

[23] Deutsche Edelstahlwerke, „Nichtrostender austenitischer Stahl 1.4404: X2CrNiMo17-12-2“. [Online]. Verfügbar unter: http://www.dew-stahl.com/fileadmin/files/dew-stahl.com/documents/Publikationen/Werkstoffdatenblaetter/RSH/1.4404_de.pdf. [Zugegriffen: 28-Apr-2016].

[24] L. Liu, J. B. Zhu, L. Li, J. C. Li, und Q. Jiang, „Microstructure and tensile properties of FeMnNiCuCoSnx high entropy alloys“, *Mater. Des.*, Bd. 44, S. 223–227, Feb. 2013.

[25] O. N. Senkov und S. L. Semiatin, „Microstructure and Properties of a Refractory High-Entropy Alloy after Cold Working“, *J. Alloys Compd.*

[26] Amco, „Mechanisch_-_physikalische_Eigenschaften_von_Alumnium_Platten“. [Online]. Verfügbar unter: http://amco-metall.de/fileadmin/downloads/Mechanisch_-_physikalische_Eigenschaften_von_Alumnium_Platten.jpg. [Zugegriffen: 28-Apr-2016].

[27] COMWORK, „LOB: Werkstoff: 3.3547“. [Online]. Verfügbar unter: http://www.lob-gmbh.de/de/werkstoffe/3.3547.html. [Zugegriffen: 28-Apr-2016].

[28] COMWORK, „LOB: Werkstoff: 3.3535“. [Online]. Verfügbar unter: http://www.lob-gmbh.de/de/werkstoffe/3.3535.html. [Zugegriffen: 28-Apr-2016].

[29] H. M. Daoud, A. M. Manzoni, N. Wanderka, und U. Glatzel, „High-Temperature Tensile Strength of Al10Co25Cr8Fe15Ni36Ti6 Compositionally Complex Alloy (High-Entropy Alloy)“, *JOM*, S. 1–7, Juni 2015.

[30] High Tech Alloys, „Hastelloy C-276“. [Online]. Verfügbar unter: http://www.hightechalloys.de/pdf/Hastelloy_C-276.pdf. [Zugegriffen: 28-Apr-2016].

References

[31] W. H. Liu, J. Y. He, H. L. Huang, H. Wang, Z. P. Lu, und C. T. Liu, „Effects of Nb additions on the microstructure and mechanical property of CoCrFeNi high-entropy alloys“, *Intermetallics*, Bd. 60, S. 1–8, Mai 2015.

[32] J. Y. He, W. H. Liu, H. Wang, Y. Wu, X. J. Liu, T. G. Nieh, und Z. P. Lu, „Effects of Al addition on structural evolution and tensile properties of the FeCoNiCrMn high-entropy alloy system“, *Acta Mater.*, Bd. 62, S. 105–113, Jan. 2014.

[33] G. A. Salishchev, M. A. Tikhonovsky, D. G. Shaysultanov, N. D. Stepanov, A. V. Kuznetsov, I. V. Kolodiy, A. S. Tortika, und O. N. Senkov, „Effect of Mn and V on structure and mechanical properties of high-entropy alloys based on CoCrFeNi system“, *J. Alloys Compd.*, Bd. 591, S. 11–21, Apr. 2014.

[34] Z. Wang, M. C. Gao, S. G. Ma, H. J. Yang, Z. H. Wang, M. Ziomek-Moroz, und J. W. Qiao, „Effect of cold rolling on the microstructure and mechanical properties of Al0.25CoCrFe1.25Ni1.25 high-entropy alloy“, *Mater. Sci. Eng. A*, Bd. 645, S. 163–169, Okt. 2015.

[35] Y. Deng, C. C. Tasan, K. G. Pradeep, H. Springer, A. Kostka, und D. Raabe, „Design of a twinning-induced plasticity high entropy alloy“, *Acta Mater.*, Bd. 94, S. 124–133, Aug. 2015.

[36] J. F. Shackelford und W. Alexander, Hrsg., *CRC Materials Science and Engineering Handbook, Third Edition*, 3 edition. Boca Raton, FL: CRC Press, 2000.

References

[37] C. Gleich GmbH, „CERTAL® hochfeste Aluminium Walzplatte“. [Online]. Verfügbar unter: http://gleich.de/de/produkte/aluminium-walzplatten/al-walzplatten---formenbau/certal?pdf. [Zugegriffen: 28-Apr-2016].

[38] Adolf Edelhoff, „Basiswerkstoffe / Technische Daten | Feindrahtwerk Adolf Edelhoff Datenblatt Cu“. [Online]. Verfügbar unter: http://www.edelhoff-wire.de/de/datenblatt-cu. [Zugegriffen: 28-Apr-2016].

[39] Y. D. Wu, Y. H. Cai, T. Wang, J. J. Si, J. Zhu, Y. D. Wang, und X. D. Hui, „A refractory Hf25Nb25Ti25Zr25 high-entropy alloy with excellent structural stability and tensile properties“, *Mater. Lett.*, Bd. 130, S. 277–280, Sep. 2014.

[40] M. J. Yao, K. G. Pradeep, C. C. Tasan, und D. Raabe, „A novel, single phase, non-equiatomic FeMnNiCoCr high-entropy alloy with exceptional phase stability and tensile ductility“, *Scr. Mater.*, Bd. 72–73, S. 5–8, Feb. 2014.

[41] Otto Fuchs, „Aluminiumlegierungen“. [Online]. Verfügbar unter: http://www.otto-fuchs.com/fileadmin/user_upload/images/pdf/Fuchs_WI_Al_D_Scr.pdf. [Zugegriffen: 28-Apr-2016].

[42] METALCOR, „2.4668 (Alloy 718), N07718 | Datenblatt | METALCOR“. [Online]. Verfügbar unter: http://www.metalcor.de/datenblatt/105/. [Zugegriffen: 28-Apr-2016].

[43] Mertens, „1.0038 / St 37-2 / S 235 JR: Datenblatt“. [Online]. Verfügbar unter: http://www.mertens-stahl.de/fileadmin/files/mertens-stahl.de/documents/Datenblaetter/Bau-_und_Qualitaetsstahl/1.0038_St37-2_S235JR__gewalzt.pdf. [Zugegriffen: 28-Apr-2016].

References

[44] C. us P. +4631 710 32 00 F. +4631 710 32 01 www arcam com S. contact form, „EBM Hardware“, *Arcam AB*. [Online]. Verfügbar unter: http://www.arcam.com/technology/electron-beam-melting/hardware/. [Zugegriffen: 27-Juli-2016].

[45] C. us P. +4631 710 32 00 F. +4631 710 32 01 www arcam com S. contact form, „Arcam A2X“, *Arcam AB*. [Online]. Verfügbar unter: http://www.arcam.com/technology/products/arcam-a2x-3/. [Zugegriffen: 27-Juli-2016].

Appendix

Density of SPS-samples

- Bestimmung mittels Archimedischer Dichtemessung

  ⇨ **ρ = 98,5 % $\rho_{theor.}$**

- Bestimmung mittels optischer Porenanalyse

  ⇨ **P = 1 %**

- Übereinstimmung mit Literaturwerten

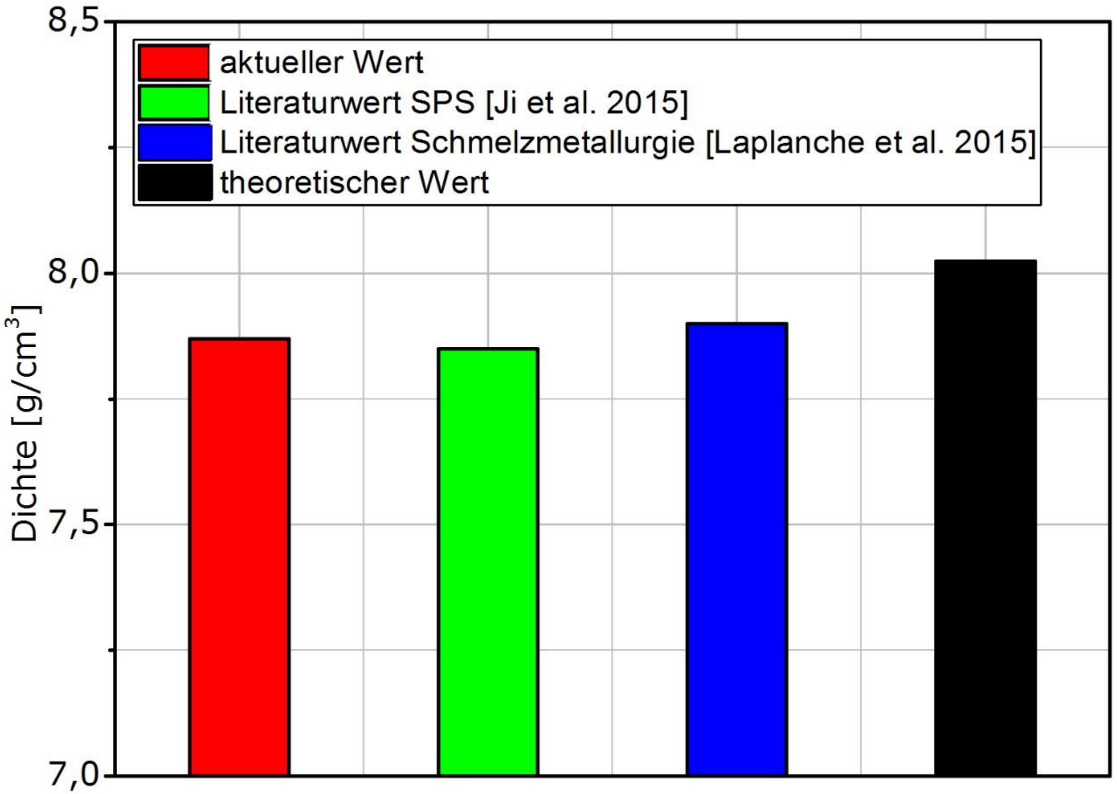

Appendix

Hardness of SPS-samples

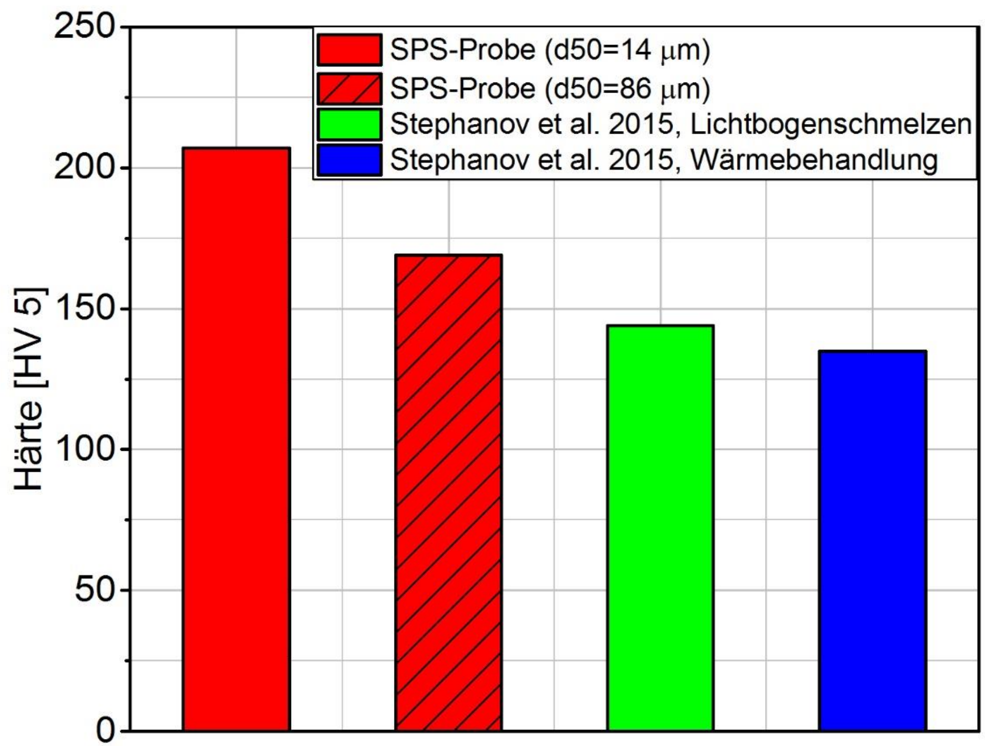

- Messung der Vickershärte
- ↓ Härtewert bei ↑ Partikelgröße
- Mittels Pulvermetallurgie höhere Härte

  ⇨ $HV = 207$ HV 5

- Wärmebehandlung geringen Einfluss
- Übereinstimmung mit Literaturwerten

Chemical composition

Probe		C [m%]	S [m%]	N [m%]	O [m%]	H [m%]
Pulver	1.Verdüsung	0,022	0,011	0,015	0,105	0,000
	1.Verdüsung, 4 Wochen an Luft			0,011	0,087	0,000
	2.Verdüsung	0,022	0,007	0,016	0,062	0,000
Fraktion	<32 µm			0,016	0,134	
	32-45 µm	-	-	0,018	0,09	0,000
	>160 µm			0,014	0,045	
Freies Sintern	Sedimentations-proben			0,034	1,16	0,099
	Pulverschüttung (<32 µm) 4 h bei 1200 °C			0,004	0,079	0,002
SPS	<32 µm	0,215	0,008	0,018	0,123	-
	63-160 µm	0,095	0,008	0,013	0,03	-